J. Phys.: Condens. Matter **21** (2009) 275407 (9pp) doi:10.1088/0953-8984/21/27/275407

A density functional study of the high-pressure chemistry of $MSiN_2$(M = Be, Mg, Ca): prediction of high-pressure phases and examination of pressure-induced decomposition

S Rebecca Römer[1], Peter Kroll[2] and Wolfgang Schnick[1]

[1] Department Chemie und Biochemie, Lehrstuhl für Anorganische Festkörperchemie, Ludwig-Maximilians-Universität München, Butenandtstraße 5-13 (D), D-81377 München, Germany
[2] Department of Chemistry and Biochemistry, University of Texas at Arlington, 700 Planetarium Place, Arlington, TX 76019-0065, USA

E-mail: wolfgang.schnick@uni-muenchen.de

Received 22 December 2008, in final form 15 April 2009
Published 12 June 2009
Online at stacks.iop.org/JPhysCM/21/275407

Abstract

Normal pressure modifications and tentative high-pressure phases of the nitridosilicates $MSiN_2$ with M = Be, Mg, or Ca have been thoroughly studied by density functional methods. At ambient pressure, $BeSiN_2$ and $MgSiN_2$ exhibit an ordered wurtzite variant derived from idealized filled β-cristobalite by a C1-type distortion. At ambient pressure, the structure of $CaSiN_2$ can also be derived from idealized filled β-cristobalite by a different type of distortion (D1-type). Energy–volume calculations for all three compounds reveal transition into an NaCl superstructure under pressure, affording sixfold coordination for Si. At 76 GPa $BeSiN_2$ forms an $LiFeO_2$-type structure, corresponding to the stable ambient-pressure modification of $LiFeO_2$, while $MgSiN_2$ and $CaSiN_2$ adopt an $LiFeO_2$-type structure, corresponding to a metastable modification (24 and 60 GPa, respectively). For both $BeSiN_2$ and $CaSiN_2$ intermediate phases appear (for $BeSiN_2$ a chalcopyrite-type structure and for $CaSiN_2$ a $CaGeN_2$-type structure). These two tetragonal intermediate structures are closely related, differing mainly in their c/a ratio. As a consequence, chalcopyrite-type structures exhibit tetrahedral coordination for both cations (M and Si), whereas in $CaGeN_2$-type structures one cation is tetrahedrally (Si) and one bisdisphenoidally (M) coordinated. Both structure types, chalcopyrite and $CaGeN_2$, can also be derived from idealized filled β-cristobalite through a B1-type distortion. The group–subgroup relation of the $BeSiN_2/MgSiN_2$, the $CaSiN_2$, the chalcopyrite, the $CaGeN_2$ and the idealized filled β-cristobalite structure is discussed and the displacive phase transformation pathways are illustrated. The zero-pressure bulk moduli were calculated for all phases and have been found to be comparable to compounds such as α-Si_3N_4, $CaIrO_3$ and Al_4C_3. Furthermore, the thermodynamic stability of $BeSiN_2$, $MgSiN_2$ and $CaSiN_2$ against phase agglomerates of the binary nitrides M_3N_2 and Si_3N_4 under pressure are examined.

S Supplementary data are available from stacks.iop.org/JPhysCM/21/275407

1. Introduction

Silicon nitride and related nitridosilicates (e.g. $\alpha/\beta/\gamma$-phases of Si_3N_4 [1–4], $M_2Si_5N_8$ (M = Ca, Sr, Ba, Eu) [5–7], $MSiN_2$ (M = Be, Mg, Ca) [8–10]) exhibit interesting and useful physical properties. Good wear resistance, high decomposition temperature, exceptional oxidation stability [11, 12], luminescence [13, 14] and nonlinear optical behaviour [15] render them interesting for industrial applications.

Throughout the last two decades, an increasing number of dense high-pressure oxosilicates have been synthesized and their material properties have been characterized [16, 17]. The high technological impact of these high-pressure silicate phases is vividly illustrated by the discovery of the extraordinary mechanical hardness of stishovite (rutile-type SiO_2) and post-stishovite (α-PbO_2 SiO_2) [18, 19]. Material properties of nitrides are often superior to those of the corresponding oxides, attributed to a higher covalency and degree of cross-linking in nitride structures [20]. Indeed, the discovery of spinel-type γ-Si_3N_4 triggered broad research efforts targeting new high-pressure nitrides and nitridosilicate with coordination behaviours of Si beyond that of a tetrahedron [3, 4].

The high-pressure behaviours of the $MSiN_2$ compounds (M = Be, Mg, Ca, Sr, Ba) is a worthwhile endeavour, since these compounds find application in several commercial/industrial processes. Moreover, they are of significant importance for the high-pressure chemistry of the prominent phosphor host lattices $M_2Si_5N_8$ (M = Ca, Sr, Ba) [21, 22]. $MgSiN_2$ is a thermally stable ceramic (up to 1400 °C [23]), and due to its wurtzite-analogous structure, discussed to substitute for AlN [24]. It is also widely used as a sintering agent and additive for Si_3N_4 ceramics [23, 25, 26]. $CaSiN_2$, besides possessing promising properties for ceramics applications [27], is an auspicious phosphor host lattice. Doped with Eu^{2+} or Ce^{3+} it is considered for use in LEDs [28, 29]. $CaSiN_2$:Ce^{3+} is one of the rare phosphor materials that can be excited by yellow-green light [29].

In this work we report on density functional calculations of ground-state structures and of several possible high-pressure phases of $BeSiN_2$, $MgSiN_2$ and $CaSiN_2$. We will illustrate their structural properties, calculate transition pressures and access their stability against decomposition into binary nitrides at elevated pressure. Results of the higher homologues, $SrSiN_2$ and $BaSiN_2$, will be reported elsewhere, as their ambient-pressure phases are structurally quite different from those of $BeSiN_2$, $MgSiN_2$ and $CaSiN_2$ [10].

2. Method

Density functional calculations [30] are performed with the Vienna *ab initio* simulation package (VASP) to obtain optimized structures, total energies and properties. VASP combines the total energy pseudopotential method with a plane-wave basis set [31–33]. The generalized gradient approximation (GGA) [34], as well as the local density approximation (LDA) for the electron exchange and correlation energy, is used and the projector-augmented-wave (PAW) method [35] is employed. We use 500 eV for the cutoff energy for the expansion of the wavefunction into the plane-wave basis set. Atomic forces are converged below 5×10^{-3} eV Å^{-1} and stresses below 0.1 GPa. The Brillouin zone is integrated by the scheme developed by Monkhorst and Pack [36].

Table 1. Calculation details.

	Formula units / cell	k-point mesh
α-$CaSiN_2$	16	$4 \times 2 \times 2$
α-$MSiN_2$ (M = Be, Mg)	4	$4 \times 4 \times 4$
β-$MSiN_2$ (M = Be, Ca) (chalcopyrite-type)	4	$5 \times 5 \times 5$
γ-$CaSiN_2$, β-$MgSiN_2$ (m-$LiFeO_2$-type)	3	$7 \times 7 \times 2$
γ-$BeSiN_2$ (s-$LiFeO_2$-type)	4	$5 \times 5 \times 4$

We made a comprehensive search of ABX_2 structure types within the international crystal structure database (ICSD). Targeting on structures with cation coordination of four and larger only, we selected more than a dozen candidate structures. These were then decorated according to the composition $MSiN_2$ and subsequently optimized in all parameters. We also invented additional structures by creating an ordered variant of AX types with high cation coordination. In total, we investigated about 20 structures—and table 1 contains only the most relevant types. While this approach is not a parameter-free global search, we are nevertheless confident that we investigate a wide variety of structural motives. Most of them are indeed observed in similar compounds (oxides).

Structural optimizations are obtained through relaxation of all structural parameters, positions as well as cell parameters. Detailed information on the cells used for calculation and the k-point meshes are given in table 1.

The GGA functional significantly better describes relative energies of structures with different coordination of the atoms. See, for instance, the pressure for the β- to γ-Si_3N_4 transition: 6 GPa are estimated using the LDA and 12.5 GPa within the GGA—with an experimental value of about 13 GPa [3]. Therefore, GGA is the better choice in comparison to the LDA for studying structural transformations at high pressure. Consequently, while we also performed all calculations using the LDA, all data reported in this work, enthalpy differences and transition pressures, are based on GGA calculations unless otherwise noted.

To obtain the zero-pressure bulk modulus, we vary the volume around the zero-pressure volume V_0. We then fit the resulting E–V data to Murnaghan's equation of state (EOS) [37] to extract the bulk modulus B_0 of a structure. We note that using Birch's or Vinet's equations of state [38, 39] give similar values. From the fitted EOS the pressure p is calculated by numerical differentiation and the enthalpy H is calculated via $H = E + pV$. Neglecting entropy effects, we choose the enthalpy difference ΔH as an appropriate measure to compare the relative stability of solid-state structures under pressure.

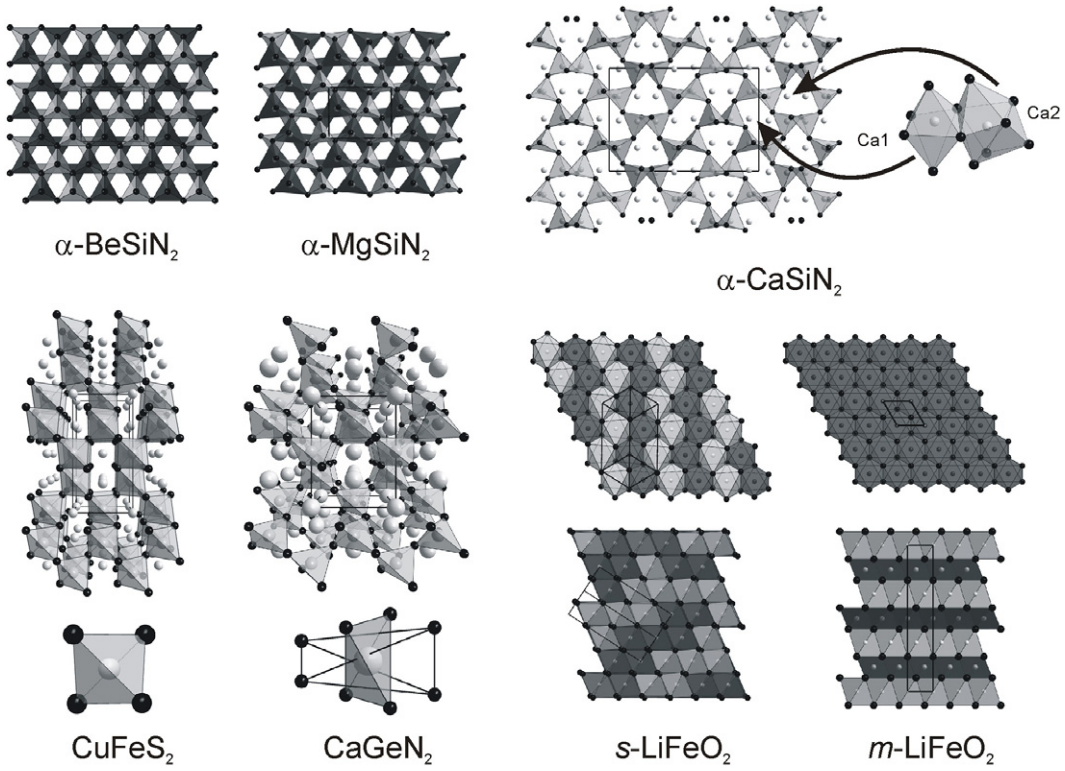

Figure 1. $MSiN_2$ structures: (1) structure of α-$BeSiN_2$ and α-$MgSiN_2$ (view along [001], MN_4 tetrahedra are depicted dark grey, SiN_4 tetrahedra light grey); (2) structure of α-$CaSiN_2$ (view along [100]; Ca atoms are depicted light grey, Si atoms dark grey, N atoms black); (3) structures of β-$BeSiN_2$ ($CuFeS_2$, c/a ratio 2.01) and β-$CaSiN_2$ ($CaGeN_2$, c/a ratio 1.36) (view along [010] with SiN_4 tetrahedra drawn; bottom BeN_4 tetrahedron and CaN_8 bisdisphenoid, respectively); (4) structures of γ-$BeSiN_2$ (s-$LiFeO_2$, top: octahedra layer, view along [0.5 0.5 0.25]; bottom: view along [−0.5 −0.5 0]) and β-$MgSiN_2$ and γ-$CaSiN_2$ (m-$LiFeO_2$, top: octahedra layer, view along [001]; bottom: view along [010]) (M = Be, Mg, Ca atoms are depicted light grey, Si atoms dark grey, N atoms black, MN_6 octahedra are depicted light grey, SiN_6 octahedra dark grey).

3. Results and discussion

3.1. $BeSiN_2$

α-$BeSiN_2$ crystallizes in an ordered wurtzite-type structure (space group $Pna2_1$, no. 33) [8], which can also be described as a C1-type distortion of the idealized filled C9 structure of β-cristobalite [40] (figure 1). We identified two candidate high-pressure structures: (I) β-$BeSiN_2$, which exhibits a chalcopyrite-like structure with tetrahedrally coordinated Be and Si (space group $I\bar{4}2d$, no. 122) [41]. This structure can be derived from β-cristobalite as well, however, in this case through a B1-type distortion [40] (figure 1). Therefore, both α- and β-$BeSiN_2$ are three-dimensional MN_4 tetrahedral networks with identical bonding topology, built up of corner-sharing tetrahedra. (II) γ-$BeSiN_2$, which adopts an $LiFeO_2$ structure (further on called s-$LiFeO_2$ as it corresponds to the stable low-temperature modification of $LiFeO_2$) with tetragonal space group $I4_1/amd$ (no. 141) [42]. It is a rock salt superstructure (doubled unit cell) and both Be and Si are octahedrally coordinated by N (figure 1). In the supplementary data (available at stacks.iop.org/JPhysCM/21/275407) we detail the crystallographic data of the three polymorphs of $BeSiN_2$ (as well as those of all later described $MSiN_2$ phases) and compare them with available experimental data. Further information on bond lengths in $BeSiN_2$ (as well as $MgSiN_2$ and $CaSiN_2$) is given in the supplementary data (available at stacks.iop.org/JPhysCM/21/275407).

Table 2. E_0, V_0, B_0 and ρ_0 for α-, β- and γ-$BeSiN_2$.

	E_0/f.u. (eV)	V_0/f.u. (10^6 pm^3)	B_0 (GPa)	ρ_0 (g cm^{-3})
α-$BeSiN_2$	−30.902	33.87	220	3.19
β-$BeSiN_2$	−30.897	33.82	222	3.20
γ-$BeSiN_2$	−28.756	28.29	244	3.82

Referring to our ambient-pressure GGA calculations, α-$BeSiN_2$ has the lowest energy of the four polymorphs (−30.902 eV/f.u.) and also the lowest density, ρ = 3.19 g cm^{-3} (exp. value 3.24 g cm^{-3} [8]). β-$BeSiN_2$ is only about 0.005 eV/f.u. higher in energy and about 0.3% denser (computed 3.20 g cm^{-3}). This result is not surprising given the close resemblance of the two modifications. γ-$BeSiN_2$ then exhibits the highest density. With ρ = 3.82 g cm^{-3} this octahedral structure is about 20% denser than both tetrahedral structures, but also about 2.1 eV per formula units higher in energy (table 2).

The zero-pressure bulk moduli of the three polymorphs are 220 GPa for α-$BeSiN_2$, 222 GPa for β-$BeSiN_2$ and 244 GPa for γ-$BeSiN_2$. Shaposhnikov *et al* [43] and Petukhov *et al* [44] report LDA values of B_0 of 264 GPa for α-$BeSiN_2$ and of 242

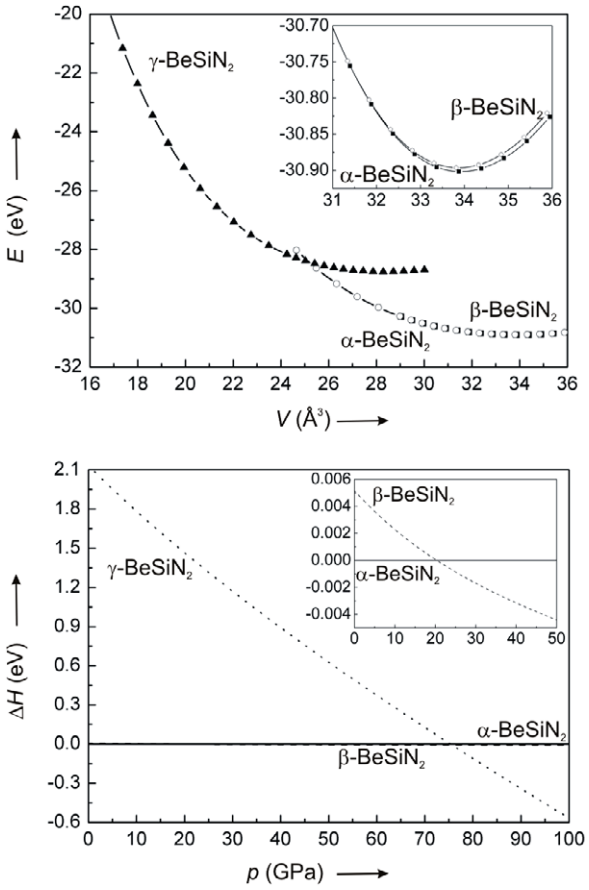

Figure 2. E–V (top) and enthalpy–pressure (bottom) diagram for all three considered phases of $BeSiN_2$ (E–V data points connected by a spline fit; enthalpy–pressure diagram from Murnaghan EOS evaluation).

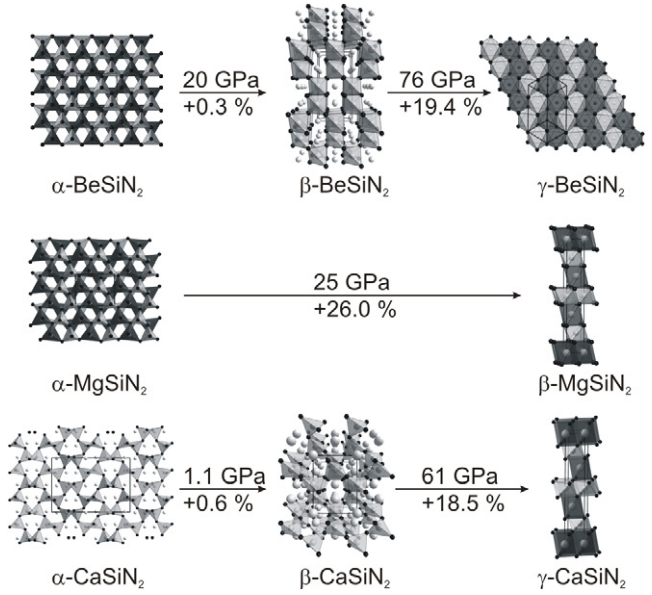

Figure 3. Sequence of structures of $BeSiN_2$, $MgSiN_2$ and $CaSiN_2$ together with transition pressures (in GPa) and values for the density increase (in percentage).

Table 3. E_0, V_0, B_0 and ρ_0 for α- and β-$MgSiN_2$.

	E_0/f.u. (eV)	V_0/f.u. (10^6pm^3)	B_0 (GPa)	ρ_0 (g cm^{-3})
α-$MgSiN_2$	−28.495	43.35	172	3.08
β-$MgSiN_2$	−27.330	34.42	223	3.88

and 240 GPa for β-$BeSiN_2$, respectively, but did not consider a γ-$BeSiN_2$. Their values match our LDA results for the bulk modulus (241 GPa for both structures). With respect to the bulk moduli, both β-$BeSiN_2$ and γ-$BeSiN_2$ are likely to be hard materials, ranking between B_4C (200 GPa) [45], α-Si_3N_4 (229 GPa) [46] and SiC (248 GPa) [45].

In figure 2 the E–V and the enthalpy–pressure curves of the three structures of $BeSiN_2$ are displayed. Apparently, α-$BeSiN_2$ is the most stable polymorph of $BeSiN_2$ for pressures up to 20 GPa, at which it will transform to β-$BeSiN_2$. Given the small enthalpy differences between α- and β-$BeSiN_2$, the actual value of the transition pressure has to be taken with care (see the inset in figure 2, bottom diagram). However, once β-$BeSiN_2$ is formed, a tetrahedral structure will remain stable up to about 76 GPa. At this pressure the structure of γ-$BeSiN_2$ with octahedral coordination becomes the most stable polymorph of $BeSiN_2$. The sequence of structures together with transition pressures and density increases is illustrated in figure 3.

3.2. $MgSiN_2$

α-$MgSiN_2$ crystallizes in the orthorhombic space group $Pna2_1$ (no. 33) and exhibits the same wurtzite-type structure as α-$BeSiN_2$ [9] (figure 1). The search for high-pressure polymorphs revealed only β-$MgSiN_2$ (figure 1) exhibiting yet another $LiFeO_2$-type structure (space group $R\bar{3}m$, no. 166, denoted m-$LiFeO_2$: this type corresponds to the metastable low-temperature modification of $LiFeO_2$ [47]). The m-$LiFeO_2$ structure can be derived from the $CdCl_2$ structure (also $R\bar{3}m$), if the unoccupied octahedral sites in $CdCl_2$ are filled with a second sort of cation. Hence, both s- and m-$LiFeO_2$ are superstructures of the rock salt structure, differing only in the ordering of cations.

Within the zero-pressure GGA calculations, the ground state of α-$MgSiN_2$ has an energy of −28.495 eV/f.u. and a density of 3.08 g cm^{-3} (exp. value: 3.13 g cm^{-3} [9]). β-$MgSiN_2$ is about 1.1 eV higher in energy than α-$MgSiN_2$ and approximately 26% denser (computed 3.88 g cm^{-3}) (table 3). The bulk modulus is 172 GPa for α-$MgSiN_2$, well within the range of previously calculated (182 GPa [48], 174 GPa [49]) and measured values (146 GPa [50], 184 GPa [51]). For β-$MgSiN_2$ we calculate a bulk modulus of 223 GPa, which is comparable to the bulk modulus of α-Si_3N_4 (220 GPa) [46].

Figure 4 then shows both the energy–volume and the enthalpy–pressure phase diagrams. Accordingly, α-$MgSiN_2$ will transform into β-$MgSiN_2$ at 25 GPa, increasing the coordination for both Mg and Si from four (tetrahedral) to six (octahedral) (figure 3).

Fang *et al* [48] reported a high-pressure transition of α-$MgSiN_2$ into a $CsICl_2$-type structure ($R\bar{3}m$, no. 166)

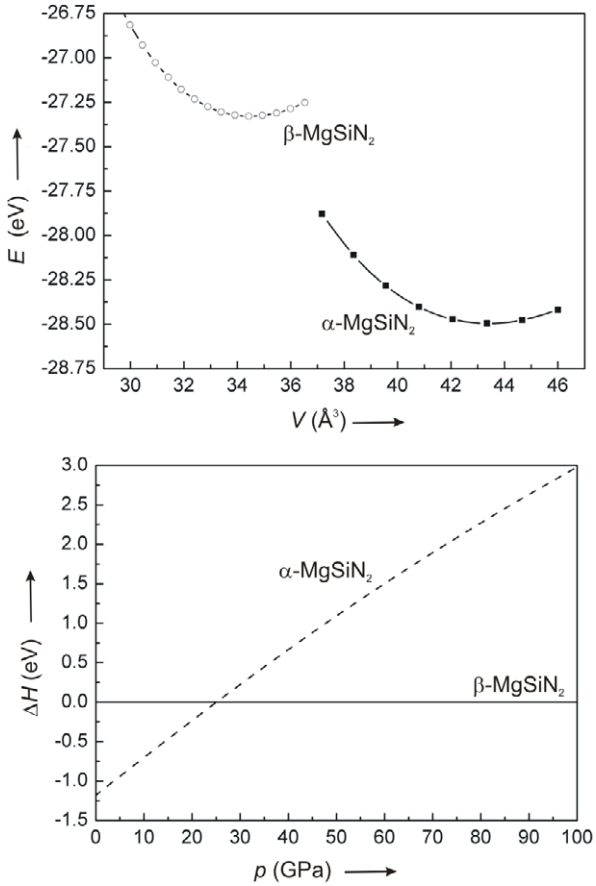

Figure 4. E–V (top) and enthalpy–pressure (bottom) diagram of the two considered phases of $MgSiN_2$ (E–V data points connected by a spline fit; enthalpy–pressure diagram from Murnaghan EOS evaluation).

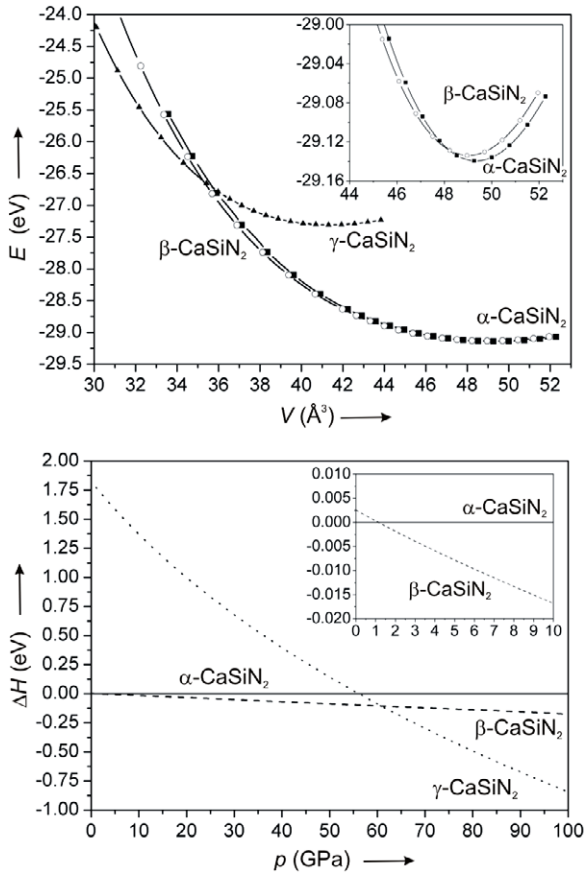

Figure 5. E–V (top) and enthalpy–pressure (bottom) diagram for all three considered phases of $CaSiN_2$ (E–V data points connected by a spline fit; enthalpy–pressure diagram from Murnaghan EOS evaluation).

and proposed a transition pressure of 16.5 GPa using LDA calculations. The lower transition pressure is explained by the choice of the different functional that artificially favours higher coordination. The structure type of $CsICl_2$ is, however, misleading. Both $CsICl_2$ and m-$LiFeO_2$ (our choice) adopt the same space group, but have very different structural parameters. In a hexagonal setting, the c/a ratios are 1.9269 for $CsICl_2$ [52] and 4.9899 for m-$LiFeO_2$ [47] (in a rhombohedral setting the rhombohedral angle is very different). As a consequence, the coordination environments are different, eightfold in $CsICl_2$ and sixfold in m-$LiFeO_2$-type. Since Fang *et al* report their optimized structure of β-$MgSiN_2$ having octahedral coordination, it is better addressed as being the m-$LiFeO_2$ structure type.

3.3. $CaSiN_2$

Ambient-pressure α-$CaSiN_2$ crystallizes in the orthorhombic space group $Pbca$ (no. 61) [10]. Corner sharing SiN_4 tetrahedra form a three-dimensional network. The structure is also related to the β-cristobalite structure (D1-type distortion of idealized C9 structure of β-cristobalite) [40]. Ca is in six- and eightfold coordination to nitrogen, respectively (figure 1). A first candidate high-pressure polymorph, β-$CaSiN_2$, is isostructural to $CaGeN_2$ [53] (B1-type distortion of the idealized filled C9 structure of β-cristobalite), which in turn is closely related to the chalcopyrite structure [41]. It crystallizes in the tetragonal space group $I\bar{4}2d$ (no. 122). Si is tetrahedrally coordinated by N. Ca exhibits a 4 + 4 bisdisphenoidal coordination. The main difference between chalcopyrite-type and $CaGeN_2$-type structures is a different c/a ratio, while the crystallographic position of atoms are quite similar. Both cations in chalcopyrite are tetrahedrally coordinated. $CaGeN_2$, on the other hand, has one cation tetrahedrally coordinated and the other in bisdisphenoidal coordination (figure 1). The second candidate structure, γ-$CaSiN_2$, again adopts an m-$LiFeO_2$-type structure (figure 1) [47].

The energy of α-$CaSiN_2$ is computed as -29.140 eV per formula unit and its density $\rho = 3.24$ g cm^{-3} (exp. value 3.30 g cm^{-3} [10]). β-$CaSiN_2$ is only slightly higher in energy, some 0.006 eV, and about 0.6% denser. γ-$CaSiN_2$ with octahedral coordination of all atoms exhibits the highest density. With $\rho = 3.87$ g cm^{-3} it is about 19% denser than both α- and β-$CaSiN_2$. The energy of γ-$CaSiN_2$ is some 1.8 eV higher than that of α-$CaSiN_2$. The zero-pressure bulk moduli of the three phases are 131 GPa, 126 GPa and 189 GPa for α-, β- and γ-$CaSiN_2$, respectively (table 4). This places them among compounds as Zr_2InC (127 GPa) [54], Al_4C_3 (130 GPa) [55] and $CaIrO_3$ (180 GPa) [56]. Along

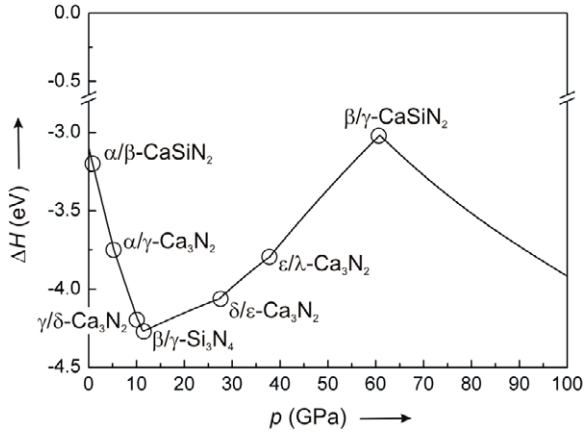

Figure 6. Enthalpy–pressure diagram for the formation of $CaSiN_2$ from Ca_3N_2 and Si_3N_4. The phase transition of β- into γ-Si_3N_4 as well as the proposed phase transformations of Ca_3N_2 (α-, γ-, δ-, ε- and λ-Ca_3N_2) have been taken into account (the pressure for each transition is indicated by a circle).

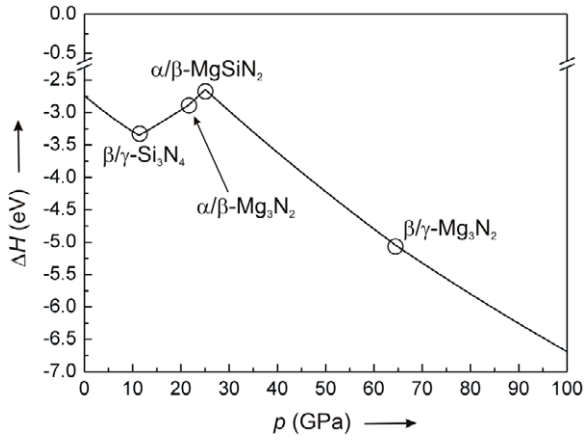

Figure 7. Enthalpy–pressure diagram for the formation of $MgSiN_2$ from Mg_3N_2 and Si_3N_4. The phase transition of β- into γ-Si_3N_4 as well as the proposed phase transformations of Mg_3N_2 (α-, β- and γ-Mg_3N_2) have been taken into account (the pressure for each transition is indicated by a circle).

the sequence $BeSiN_2$, $MgSiN_2$ and $CaSiN_2$, therefore, $CaSiN_2$ phases show the lowest bulk moduli.

Interestingly, when calculating $CaSiN_2$ in the $MgSiN_2$-type structure [9], we obtained an even lower energy than that computed for α-$CaSiN_2$. The energy difference, a tiny 0.001 eV, however, is very small, and well within possible entropy effects or even within a systematic error of DFT calculations. Employing LDA calculations, on the other hand, places the α-$CaSiN_2$ 0.032 eV below the $MgSiN_2$ type.

Energy–volume and enthalpy–pressure phase diagrams of $CaSiN_2$ are shown in figure 5. Accordingly, we find a first transition of α-$CaSiN_2$ into β-$CaSiN_2$ already at 1.1 GPa. β-$CaSiN_2$ will be the most stable polymorph up to 61 GPa, when the structure of γ-$CaSiN_2$ with all-octahedral coordination is adopted. The sequence of the structures is illustrated in figure 3.

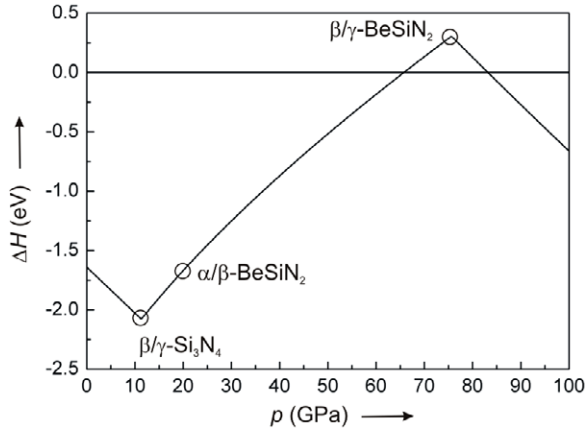

Figure 8. Enthalpy–pressure diagram for the formation of $BeSiN_2$ from Be_3N_2 and Si_3N_4. The phase transition of β- into γ-Si_3N_4 has been taken into account (no phase transformations of Be_3N_2 are found up to 100 GPa) (the pressure for each transition is indicated by a circle).

Table 4. E_0, V_0, B_0 and ρ_0 for α-, β-, γ-$CaSiN_2$ and $CaSiN_2$ in the $MgSiN_2$ structure.

	E_0/f.u. (eV)	V_0/f.u. (10^6 pm^3)	B_0 (GPa)	ρ_0 (g cm^{-3})
α-$CaSiN_2$	−29.140	49.26	131	3.24
β-$CaSiN_2$	−29.134	48.96	126	3.26
γ-$CaSiN_2$	−27.309	41.31	189	3.87
'$MgSiN_2$'	−29.141	50.64	121	3.15

3.4. Thermodynamic stability of $MSiN_2$ at high pressure

Finally, we access the thermodynamic stability of $MSiN_2$ compounds versus a phase agglomerate of M_3N_2 (M = Ca, Mg) and Si_3N_4. To achieve this, we took all known high-pressure phases of Ca_3N_2 [57], Mg_3N_2 [58] and Si_3N_4 [3, 4] into account (figures 6 and 7). We find that both the ternary phases of $CaSiN_2$ and $MgSiN_2$ are always lower in enthalpy than a mixture of the two binary phases M_3N_2 (M = Ca, Mg) and Si_3N_4. This opens up another possible synthesis route for $CaSiN_2$ and $MgSiN_2$ and its high-pressure phases, as they should be attainable under high pressure starting from Si_3N_4 and Ca_3N_2 or Mg_3N_2, respectively. High temperatures should accompany the high-pressure syntheses to overcome high activation barriers due to strong bonds in and low interdiffusion coefficients of Si_3N_4 and Ca_3N_2/Mg_3N_2.

$BeSiN_2$, on the other hand, is stable against decomposition only up to 66 GPa, at which pressure a phase agglomerate of Be_3N_2 and Si_3N_4 is more favourable. Interestingly, above 83 GPa $BeSiN_2$ should reappear, adopting the γ-$BeSiN_2$ structure (figure 8). Consequently, γ-$BeSiN_2$ will be attainable only above 83 GPa, possibly from the binary nitrides.

4. Conclusion

The structures of α-$MSiN_2$ (M = Be, Mg, Ca), β-$BeSiN_2$ and β-$CaSiN_2$ are related to the filled β-cristobalite structure (filled C9 structure) by group–subgroup relations (figure 9). They

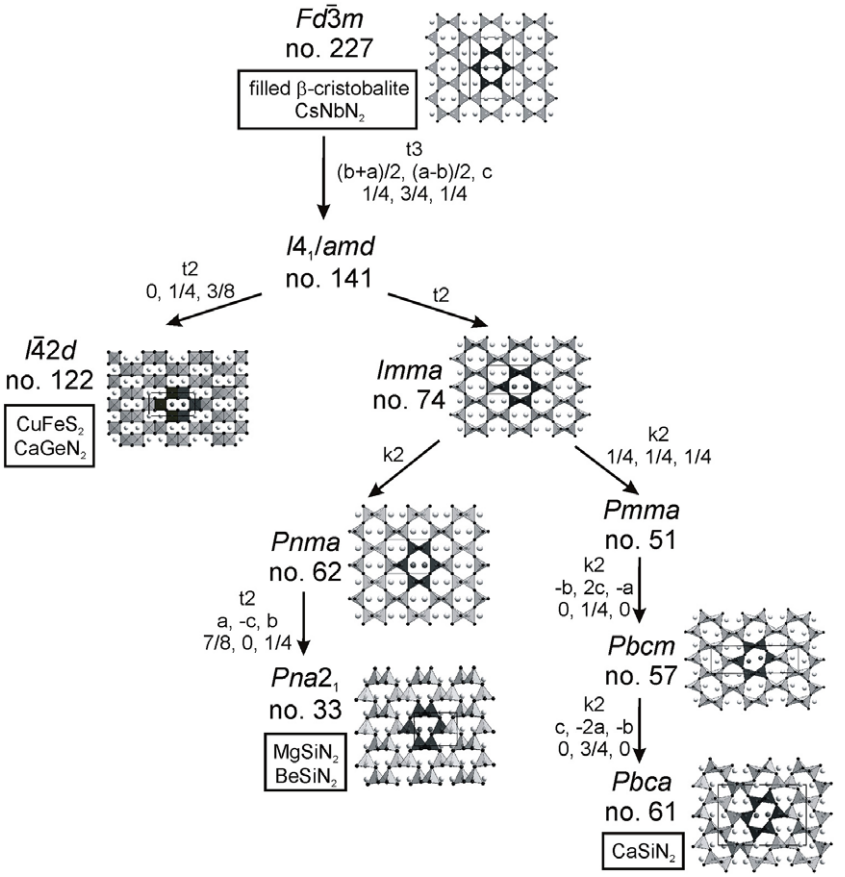

Figure 9. Group–subgroup schema for the relation of the α-$MSiN_2$ (M = Be, Mg, Ca) and the β-$MSiN_2$ (M = Be, Ca) structures to the filled β-cristobalite structure.

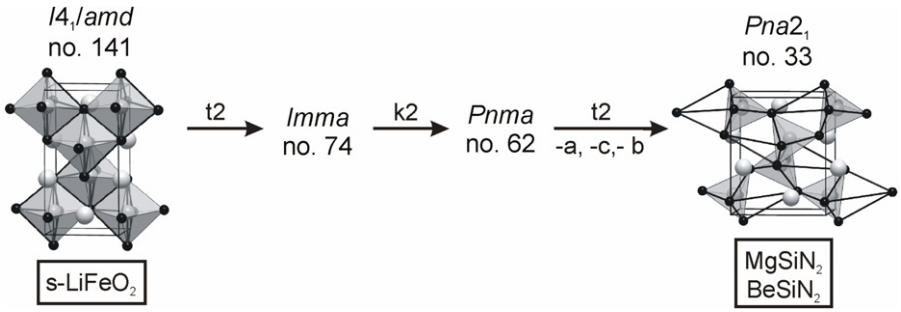

Figure 10. Group–subgroup scheme for s-$LiFeO_2$ and $BeSiN_2$/$MgSiN_2$. Both structures are presented in equivalent detail and the polyhedra of the partner structure are enhanced by thick black lines, respectively.

derive from the parent structure (space group $Fd\bar{3}m$, no. 227) by concerted rotations of tetrahedra (for a detailed discussion on these rotation patterns see the works of Thompson *et al* [40] and O'Keeffe and Hyde [59]). Hence, displacive phase transition pathways are conceivable for α-$BeSiN_2$ ($Pna2_1$) into β-$BeSiN_2$ ($I\bar{4}2d$) and for α-$CaSiN_2$ ($Pnma$) into β-$CaSiN_2$ ($I\bar{4}2d$). This might well result in quite low activation energy barriers for these two phase transitions.

The structures of γ-$BeSiN_2$ ($I4_1/amd$, s-$LiFeO_2$), β-$MgSiN_2$ ($R\bar{3}m$, m-$LiFeO_2$) and γ-$CaSiN_2$ ($R\bar{3}m$, m-$LiFeO_2$) are all related to the rock salt structure. The difference between the s- and m-$LiFeO_2$-type structures is a different ordering of the two types of cations on octahedral sites. In m-$LiFeO_2$ layers of condensed LiO_6 octahedra alternate with layers of condensed FeO_6 octahedra. In s-$LiFeO_2$ structures every layer is occupied half by Li and half by Fe. The s-$LiFeO_2$-type structure seems to be preferred for compounds, with both cations having approximately the same size as in $BeSiN_2$ ($r(Be^{2+}) = 59$ [60], 31 pm [61]; $r(Si^{4+}) = 54$ [60], 29 pm [61]). If the two cations differ substantially in size as in $MgSiN_2$ and $CaSiN_2$ ($r(Mg^{2+}) = 86$ [60], 70 pm [61]; $r(Ca^{2+}) = 114$ [60], 105 pm [61]), the m-$LiFeO_2$-type structure is favoured, as the height of the octahedral layers can be adjusted to the size of the cation occupying it.

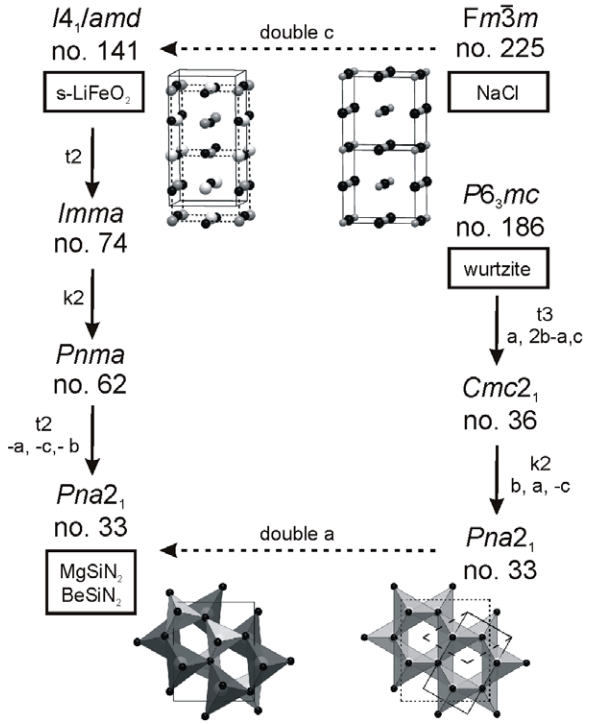

Figure 11. Relation of the NaCl structure to the s-$LiFeO_2$ structure and of the wurtzite (ZnS) structure to the $BeSiN_2$ and $MgSiN_2$ structure (pictures: s-$LiFeO_2$: double unit cell of NaCl drawn in addition to the tetragonal unit cell; wurtzite: unit cell of wurtzite drawn as well as of wurtzite reduced to $Pna2_1$ and of $BeSiN_2$ and $MgSiN_2$).

The s-$LiFeO_2$ structure adopted by $BeSiN_2$ (γ-phase) is related to α-$BeSiN_2$ (and α-$MgSiN_2$) through a group–subgroup relation (figure 10). Simply put, by compressing α-$BeSiN_2$ along two unit cell axes and simultaneously elongating the third (corresponding to the c axis in tetragonal s-$LiFeO_2$), the distorted hexagonal close packing (hcp) of the anions in α-$BeSiN_2$ is transformed into a cubic close packing (ccp, distorted as well) and the cations are transferred from the tetrahedral sites in hcp to the octahedral sites in ccp by only a small movement. This transformation is analogous to the well-known wurtzite–rock salt transition [62]. α-$BeSiN_2$ exhibits an ordered wurtzite structure and s-$LiFeO_2$ the corresponding ordered rock salt structure (compare figure 11), only that the ordering of the cations results in a doubled unit cell for s-$LiFeO_2$ and α-$BeSiN_2$ if compared to the rock salt and wurtzite structure, respectively. However, as wurtzite-type $BeSiN_2$ might transform first into a $CuFeS_2$-type structure according to the enthalpy–pressure phase diagram (figure 2), which is not related to the s-$LiFeO_2$-type structure, it is unclear whether a displacive phase transition along the wurtzite–rock salt transformation pathway will take place. The m-$LiFeO_2$-type structure, while also exhibiting an ordered rock salt superstructure, is not related to either of the discussed structures.

It has to be noted that the s-$LiFeO_2$ structure ($I4_1/amd$) is not related to the filled β-cristobalite structure, even though the space group sequence $I4_1/amd$ to $Pna2_1$ is identical to that of filled β-cristobalite $I4_1/amd$ to $Pna2_1$. In filled β-cristobalite, reduced to $I4_1/amd$, the X atoms of ABX_2 occupy the 8c positions whereas in s-$LiFeO_2$ they occupy the 8e positions.

5. Summary

We investigated the pressure-dependent phase diagrams of the nitridosilicates $MSiN_2$ (M = Be, Mg, Ca). For $BeSiN_2$ two candidate structures, a $CuFeS_2$-type (β-$BeSiN_2$) and a s-$LiFeO_2$-type (γ-$BeSiN_2$) were found to become lower in enthalpy at high pressure than the α phases. For $MgSiN_2$, an m-$LiFeO_2$-type (β-$MgSiN_2$) will appear at high pressures. For $CaSiN_2$ we found two potential high-pressure phases, a $CaGeN_2$-type (β-$CaSiN_2$) and a m-$LiFeO_2$-type (γ-$CaSiN_2$). In each system, the phases most stable at very high pressure—γ-$BeSiN_2$, β-$MgSiN_2$ and γ-$CaSiN_2$—exhibit ordered rock salt structures with octahedral coordination of Si. The calculated bulk moduli indicate an increase in hardness for these high-pressure phases. We found that $CaSiN_2$ and $MgSiN_2$ are thermodynamically stable against decomposition into the binary nitrides up to 100 GPa. $BeSiN_2$ exhibits a 'stability gap' between 66 and 83 GPa. In this pressure region a phase assemblage of Be_3N_2 and Si_3N_4 is more favourable.

Acknowledgments

Financial support by the Deutsche Forschungsgemeinschaft, (priority programme SPP 1236, project SCHN 377/13 and Kr 1805/10 and Heisenberg-programme Kr 1805/9) as well as the Fonds der Chemischen Industrie (FCI), Germany, is gratefully acknowledged. The authors would further like to thank the Leibniz Rechenzentrum, Munich for computational resources on the Linux Cluster System, as well as the Texas Advanced Computing Center at Austin.

References

[1] Ruddlesden S N and Popper P 1958 *Acta Crystallogr.* **11** 465
[2] Hardie D and Jack K H 1957 *Nature* **180** 332
[3] Zerr A, Miehe G, Serghiou G, Schwarz M, Kroke E, Riedel R, Fueß H, Kroll P and Boehler R 1999 *Nature* **400** 340
[4] Schwarz M, Miehe G, Zerr A, Kroke E, Poe B T, Fuess H and Riedel R 2000 *Adv. Mater.* **12** 883
[5] Schlieper T and Schnick W 1995 *Z. Anorg. Allg. Chem.* **621** 1037
[6] Schlieper T, Milius W and Schnick W 1995 *Z. Anorg. Allg. Chem.* **621** 1380
[7] Huppertz H and Schnick W 1997 *Acta Crystallogr.* C **53** 1751
[8] Eckerlin P 1967 *Z. Anorg. Allg. Chem.* **353** 225
[9] David J, Laurent Y and Lang J 1970 *Bull. Soc. Fr. Minéral. Cristallogr.* **93** 153
Wintenberger M, Tcheou F, David J and Lang J 1980 *Z. Naturf.* B **35** 604
[10] Gál Z A, Mallinson P M, Orchard H J and Clarke S J 2004 *Inorg. Chem.* **43** 3998
[11] Hampshire S 1994 *Materials Science and Technology* vol 11, ed R W Cahn, P Haasen and E J Kramer (Weinheim: Wiley–VCH)
[12] Nordberg L-O, Nygren M, Käll P-O and Shen Z 1998 *J. Am. Ceram. Soc.* **81** 1461

[13] Mueller-Mach R, Mueller G, Krames M R, Höppe H A, Stadler F, Schnick W, Juestel T and Schmidt P 2005 *Phys. Status Solidi* a **202** 1727
[14] Jüstel T, Nikol H and Ronda C 1998 *Angew. Chem.* **110** 3250
Jüstel T, Nikol H and Ronda C 1998 *Angew. Chem. Int. Edn* **37** 3084
[15] Lutz H, Joosten S, Hoffmann J, Lehmeier P, Seilmeier A, Höppe H A and Schnick W 2004 *J. Phys. Chem. Solids* **65** 1285
[16] Finger L W and Hazen R M 2001 *Rev. Mineral. Geochem.* **41** 123
[17] Hazen R M, Downs R T and Finger L W 1996 *Science* **272** 1769
[18] Dubrovinskaia N and Dubrovinsky L S 2001 *Mater. Chem. Phys.* **68** 77
[19] Leger J M, Haines J, Schmidt M, Petitet J P, Pereira A S and da Jornada J A H 1996 *Nature* **383** 401
[20] Schnick W 1993 *Angew. Chem.* **105** 846
Schnick W 1993 *Angew. Chem. Int. Edn Engl.* **32** 806
[21] Römer S R, Braun C, Oeckler O, Schmidt P, Kroll P and Schnick W 2008 *Chem. Eur. J.* **14** 7892
[22] Römer S R 2009 *Dissertation* Ludwig-Maximilians-University Munich
[23] Lences Z, Hirao K, Sajgalik P and Hoffmann M J 2006 *Key Eng. Mater.* **317/318** 857
[24] Peng L, Xu L, Zhicheng J, Zhang J, Yang J and Qian Y 2008 *Commun. Am. Ceram. Soc.* **91** 333
[25] Peng G, Jiang G, Li W, Zhang B and Chen L 2006 *J. Am. Ceram. Soc.* **89** 3824
[26] Peng G, Jiang G, Zhuang H, Li W and Xu S 2005 *Mater. Res. Bull.* **40** 2139
[27] Groen W A, Kraan M J and de With G 1994 *J. Mater. Sci.* **29** 3161
[28] Lee S S, Lim S, Sun S S and Wager J F 1997 *Proc. SPIE—Int. Soc. Opt. Eng.* **3241** 75
[29] Le Toquin R and Cheetham A K 2006 *Chem. Phys. Lett.* **423** 352
[30] Hohenberg P and Kohn W 1964 *Phys. Rev.* B **136** 864
[31] Kresse G and Hafner J 1993 *Phys. Rev.* B **47** 558
Kresse G and Hafner J 1994 *Phys. Rev.* B **49** 14251
[32] Kresse G and Furthmüller J 1996 *Comput. Mater. Sci.* **6** 15
[33] Kresse G and Furthmüller J 1996 *Phys. Rev.* B **54** 11169
[34] Perdew J P 1991 *Electronic Structures of Solids '91* ed P Ziesche and H Eschrig (Berlin: Akademie Verlag)
[35] Kresse G and Joubert J 1999 *Phys. Rev.* B **59** 1758
[36] Monkhorst H J and Pack J D 1976 *Phys. Rev.* B **13** 5188
[37] Murnaghan F D 1944 *Proc. Natl Acad. Sci. USA* **30** 244
[38] Birch F 1952 *J. Geophys. Res.* **57** 227
[39] Vinet P, Ferrante J, Smith J R and Rose J H 1987 *Phys. Rev.* B **35** 1945
Vinet P, Rose J H, Ferrante J and Smith J R 1989 *J. Phys.: Condens. Matter* **1** 1941
[40] Thompson J G, Withers R L, Palethorpe S R and Melnitchenko A 1998 *J. Solid State Chem.* **141** 29
[41] Pauling L and Brockway L O 1932 *Z. Kristallogr. Kristallgeom. Kristallphys. Kristallchem.* **82** 188
[42] Cox D E, Takei W J and Shirane G 1962 *Am. Crystallogr. Assoc.* **1962P** 6
[43] Shaposhnikov V L, Krivosheeva A V, D'Avitaya F A, Lazzari J-L and Borisenko V E 2008 *Phys. Status Solidi* b **245** 142
[44] Petukhov A G, Lambrecht W R L and Segall B 1994 *Phys. Rev.* B **49** 4549
[45] Ahuja R and Dubrovinsky L S 2002 *J. Phys.: Condens. Matter* **14** 10995
[46] Kruger M B, Nguyan J H, Li Y M, Caldwell W A, Manghnani M H and Jeanloz R 1997 *Phys. Rev.* B **55** 3456
[47] Douakha N, Holzapfel M, Chappel E, Chouteau G, Croguennec L, Ott A and Ouladdiaf B 2002 *J. Solid State Chem.* **163** 406
[48] Fang C M, Hintzen H T and de With G 2004 *Appl. Phys.* A **78** 717
[49] Huang J Y, Tang L-C and Lee M H 2001 *J. Phys.: Condens. Matter* **13** 10417
[50] Groen W A, Kaan M J and de With G 1993 *J. Eur. Ceram. Soc.* **12** 413
[51] Bruls R J 2000 *PhD Thesis* University of Eindhoven
[52] Wyckoff R W G 1920 *J. Am. Chem. Soc.* **42** 1100
[53] Maunaye M, Guyader J, Laurent Y and Lang J 1971 *Bull. Soc. Fr. Minéral. Cristallogr.* **94** 347
[54] Manoun B, Saxena S K, Liermann H P, Gulve R P, Hoffman E, Asrsoum M W, Hug G and Zha C S 2004 *Appl. Phys. Lett.* **85** 1514
[55] Solozhenko V L and Kurakevych O O 2005 *Solid State Commun.* **133** 385
[56] Martin C D, Chapman K W, Chupas P J, Prakapenka V, Lee P L, Shastri S D and Parise J B 2007 *Am. Mineral.* **92** 1048
[57] Römer S R, Schnick W and Kroll P 2009 *J. Phys. Chem.* C **113** 2943
[58] Römer S R, Kroll P and Schnick W 2009 *Phys. Status Solidi* b at press (doi:10.1002/pssb.200945011)
[59] O'Keeffe M and Hyde B G 1976 *Acta Crystallogr.* B **32** 2923
[60] Shannon R D 1976 *Acta Crystallogr.* A **32** 751
[61] Baur W H 1987 *Crystallogr. Rev.* **1** 59
[62] Desgreniers S 1998 *Phys. Rev.* B **58** 14102
Sharma S M and Gupta Y M 1998 *Phys. Rev.* B **58** 5964
Perlin P, Jauberthie-Carillon C, Itie J P, Miguel A S, Grzegory I and Polian A 1992 *Phys. Rev.* B **45** 83
Xia H, Xia Q and Ruoff A L 1993 *Phys. Rev.* B **47** 12925
Ueno M, Yoshida M, Onodera A, Shimomura O and Takemura K 1994 *Phys. Rev.* B **49** 14
Ueno M, Onodera A, Shimomura O and Takemura K 1992 *Phys. Rev.* B **45** 10123
Perlin P, Jauberthie-Carillon C, Itie J P, San Miguel A, Grzegory I and Polian A 1991 *High Pressure Res.* **7** 96
Perlin P, Gorczyca I, Porowski S, Suski T, Christensen N E and Polian A 1993 *Japan. J. Appl. Phys. Suppl.* **32** 135
Uehara S, Masamoto T, Onodera A, Ueno M, Shimomura O and Takemura K 1997 *J. Phys. Chem. Solids* **58** 2093